THE JOURNAL OF BIOLOGICAL CHEMISTRY
Vol. 275, No. 31, Issue of August 4, pp. 23933–23938, 2000

Printed in U.S.A.

Manganese Selectivity of Pmr1, the Yeast Secretory Pathway Ion Pump, Is Defined by Residue Gln^{783} in Transmembrane Segment 6

RESIDUE Asp^{778} IS ESSENTIAL FOR CATION TRANSPORT*

Received for publication, March 28, 2000, and in revised form, April 27, 2000
Published, JBC Papers in Press, May 5, 2000, DOI 10.1074/jbc.M002619200

Debjani Mandal, Thomas B. Woolf, and Rajini Rao‡

From the Department of Physiology, The Johns Hopkins University School of Medicine, Baltimore, Maryland 21205

We have solubilized and purified the histidine-tagged yeast secretory pathway/Golgi ion pump Pmr1 to near homogeneity in one step, using nickel affinity chromatography. The purified pump demonstrates both Ca^{2+}- and Mn^{2+}-dependent ATP hydrolysis and phosphoenzyme intermediate formation in forward (ATP) and reverse (P_i) directions. This preparation has allowed us to examine, in detail, the properties of mutations D778A and Q783A in transmembrane segment M6 of Pmr1. In phenotypic screens of Ca^{2+} chelator and Mn^{2+} toxicity reported separately (Wei, Y., Chen, J., Rosas, G., Tompkins, D.A., Holt, P.A., and Rao, R. (2000) J. Biol. Chem. 275, XXXX–XXXX), D778A was a loss-of-function mutant apparently defective for transport of both Ca^{2+} and Mn^{2+}, whereas mutant Q783A displayed a differential sensitivity consistent with the selective loss of Mn^{2+} transport. We show that mutant D778A is devoid of cation-dependent ATP hydrolytic activity and phosphoenzyme formation from ATP. However, reverse phosphorylation from P_i is preserved but is insensitive to inhibition by Ca^{2+} or Mn^{2+} ions, which is evidence for a specific inability to bind cations in this mutant. We also show that Ca^{2+} can activate ATP hydrolysis in the purified Q783A mutant, with a half-maximal concentration of 0.06 μM, essentially identical to that of wild type (0.07 μM). Mn^{2+} activation of ATP hydrolysis was half-maximal at 0.02 μM in wild type, establishing a normal selectivity profile of $Mn^{2+} > Ca^{2+}$. Strikingly, Mn^{2+}-ATPase in the Q783A mutant was nearly abolished, even at concentrations of up to 10 μM. These results were confirmed in assays of phosphoenzyme intermediates. Molecular modeling of the packing between helices M4 and M6 suggests that residue Gln^{783} in M6 may form a critical hydrophobic interaction with Val^{335} in M4, such that the Ala substitution modifies the packing or tilt of the helices and thus the ion pore. The data emphasize the critical role of transmembrane segment M6 in defining the cation binding pocket of P-type ATPases.

In recent years, there has been a growing awareness of Mn^{2+} as an effective surrogate for Ca^{2+} in supporting cell growth (1, 2). The ionic radius and coordination chemistry of Mn^{2+} is closer to that of Ca^{2+} than other physiological cations, and both Ca^{2+} and Mn^{2+} bind to oxygen- and nitrogen-based ligands on proteins (3–6). Support for speculation that Mn^{2+} and Ca^{2+} can function interchangeably in signal transduction comes from observations that Mn^{2+} can replace Ca^{2+} in a number of well established signaling systems, including calmodulin activation (7), cyclic nucleotide metabolism (8), and secretion (9). In yeast, free Mn^{2+} was shown to be 500–1000-fold more effective than free Ca^{2+} in supporting bud development and cell cycle progression (1). Manganese is believed to be abundantly available in the natural habitat of yeast, at an estimated concentration of 100 μM in rotting vegetation (6, 10), and may well play a physiologically relevant role in mediating cell growth. Thus, the mobilization and transport of Mn^{2+} are likely to emulate that of Ca^{2+} (11).

The yeast ion pump Pmr1, which localizes to the medial Golgi, has been implicated in the delivery of both Ca^{2+} and Mn^{2+} to the secretory pathway (2, 12), where they have distinct roles in sustaining protein sorting (Ca^{2+}) or protein glycosylation (Mn^{2+}). Cytosolic Mn^{2+} accumulates in *pmr1* mutants and can serve as an inorganic scavenger of superoxide radicals, thus bypassing the requirement for cytosolic superoxide dismutase in aerobic growth (12). Consequently, *pmr1* mutants also display hypersensitivity to the growth toxicity of millimolar concentrations of extracellular Mn^{2+}, indicating that delivery into the secretory pathway by Pmr1, and subsequent exocytosis, must be a major route for cellular detoxification of Mn^{2+}. In earlier work, we have demonstrated that Mn^{2+} is a potent inhibitor of Pmr1-mediated $^{45}Ca^{2+}$ transport in isolated Golgi vesicles, consistent with competition for transport sites (13).

In the accompanying work (14), we have taken advantage of the hypersensitivity of the *pmr1* null strain to BAPTA[1] and Mn^{2+} toxicity and screened for mutants defective in cation transport and selectivity (14). The identification of the mutation Q783A in transmembrane segment M6 of Pmr1, which conferred hypersensitivity to Mn^{2+} toxicity but retained normal ^{45}Ca transport characteristics, provided a preliminary insight into the molecular basis of ion selectivity in transport ATPases (14). Several loss-of-function mutants, resembling the null strain in both BAPTA and Mn^{2+} hypersensitivity, were also identified. One such mutant, D778A, again in M6, retained normal biogenesis and ATP binding ability but had no detectable transport activity (14). This residue is conserved in all Pmr1 homologues sequenced to date and likely contributes

* This work was supported by American Cancer Society Grants IRG11-33 and JFRA 538, American Heart Association Grant-In-aid 95012290, and National Institutes of Health Grant GM52414 (to R. R.). The costs of publication of this article were defrayed in part by the payment of page charges. This article must therefore be hereby marked "*advertisement*" in accordance with 18 U.S.C. Section 1734 solely to indicate this fact.

‡ To whom correspondence should be addressed: Dept. of Physiology, Johns Hopkins University School of Medicine, 725 N. Wolfe St., Baltimore MD 21205. Tel.: 410-955-4732; Fax: 410-955-0461; E-mail: rrao@jhmi.edu.

[1] The abbreviations used are: BAPTA, 1,2-bis(2-aminophenoxy)-ethane-*N*,*N*,*N*′,*N*′-tetraacetic acid; PAGE, polyacrylamide gel electrophoresis; SERCA, sarco/endoplasmic reticulum Ca^{2+}-ATPase; Ni-NTA, nickel-nitrilotriacetic acid.

directly to cation binding, analogous to the proposed role of the equivalent aspartate in SERCA and the Na^+/K^+-ATPase (15, 16). Here, we describe the solubilization and purification of His-tagged Pmr1, by nickel affinity chromatography. The purified preparations were used to assay cation-dependent ATP hydrolysis and phosphoenzyme formation in wild type and mutants D778A and Q783A. The data support a critical role for Asp^{778} in the cation-binding pocket and demonstrate a striking reversal in ion selectivity for the Q783A mutant. The phenotype of additional substitutions at residue 783 have led us to hypothesize a role for this residue in M4-M6 helix packing, which is supported by molecular modeling simulation.

EXPERIMENTAL PROCEDURES

Media, Strains, and Plasmids

Cultures were grown in defined minimal media containing yeast nitrogen base (6.7 g/liter; Difco), dextrose (2%), and supplements as needed. Growth assays in BAPTA- and Mn^{2+}-supplemented medium were done exactly as described (14). Yeast strain K616 (Δ*pmr1*Δ*pmc1*Δ*cnb1*) was used as host and has been described before (17). Plasmid YCpHR1 is a centromeric yeast plasmid carrying the *PMR1* gene under heat shock control (14). Mutations Q783A and D778A were made earlier (14); additional substitutions of Gln^{783} with Leu, Glu, Thr, Asn, Ser, and Cys were made by the "inverse polymerase chain reaction" method using a pair of oligonucleotides in each case (18). Mutations were confirmed by DNA sequencing and introduced into plasmid YCpHR1 by standard cloning techniques. Plasmid YEpHis-PMR1 is a 2μ plasmid expressing the N-terminal His_9-tagged Pmr1 behind the constitutive *PGK* promoter and has been described earlier (13). Briefly, it was constructed by replacing the initiator ATG codon in *PMR1* with a unique *Mlu*I site and cloning into the expression vector pSM1052 (gift of Susan Michaelis, Johns Hopkins University). This construct results in a 15-residue N-terminal extension of Pmr1 having the sequence RGSQHHHHHHHHHTR following the initiating Met. Mutations Q783A and D778A were introduced into YEpHisPMR1 by cloning a 3-kilobase pair *Bam*HI fragment containing the mutation from the YEpHR1 construct (14) and verifying correct orientation by restriction analysis.

Solubilization and Purification of Histidine-tagged Pmr1

Isolation of Golgi membranes by sucrose density gradient centrifugation of clarified yeast lysates was exactly as described earlier (19). A crude detergent extract was prepared by suspending 1 mg of Golgi membranes in 1 ml of solubilization buffer *S* containing 20 mM Hepes/Tris, pH 7.0, 20% glycerol, 0.5% *Escherichia coli* total lipid extract, 1.5% *n*-octyl-β-D-glucopyranoside, 6 mM β mercaptoethanol, and protease inhibitors (20). The resulting suspension was mixed for 2 h on a rotary motor at 4 °C. The mixture was cleared of unextractable materials by centrifugation at 100,000 × *g* for 1 h at 4 °C.

Meanwhile, 0.1 ml of bed volume of Ni-NTA-agarose (Qiagen) was placed in a 2-ml microcentrifuge tube and washed twice with 0.5 ml of cold water and washed twice with 1 ml of buffer *S* plus 10 mM imidazole. The detergent extract was added to the equilibrated resin and incubated at 4 °C for 2.5 h with gentle shaking. The mixture was then transferred to a 2-ml Micro Bio-Spin column (Bio-Rad), and unbound material was collected by gravity elution. The column was washed with 20 column volumes of Wash Buffer (Buffer *S* plus 200 mM NaCl and 50 mM imidazole) to release nonspecifically bound material. His_9-Pmr1 was eluted following incubation with 0.2–0.3 ml of elution buffer (Buffer *S* plus 300 mM imidazole) for 5 min. The eluted material was collected by centrifugation at 1000 × *g* for 30 s in a refrigerated microcentrifuge, immediately frozen in a dry ice/ethanol bath, and stored at −80 °C until further use.

[γ-^{32}P]ATP Hydrolysis

The method of Ghosh *et al*. (21) was followed, with some modifications. Here, the assay mixture was reduced to 0.1 ml and contained 50 mM Hepes/Tris, pH 7.0, 100 mM KCl, and 1 mM $MgCl_2$. Cations (Ca^{2+} and Mn^{2+}) were added as the chloride salts and buffered with EGTA as specified in the figure legends; free cation concentration was determined by the WinMaxChelator computer program (22). Ni-NTA eluted Pmr1 (1 μg) was preincubated in the reaction mixture at room temperature, and ATP hydrolysis was initiated by the addition of 5 μl of 1 mM [γ-^{32}P]ATP (3000 Ci/mmol; Amersham Pharmacia Biotech) to a final concentration of 50 μM (500–600 cpm/pmol). After the desired incubation period, the reaction was terminated with 10 μl of 25% trichloroacetic acid, followed by the addition of 10 μl of 100 mM KH_2PO_4. Then 0.1 ml of a suspension of activated charcoal (1:1 in water; Sigma) was added. After mild stirring for 10 min, the charcoal was precipitated by centrifugation in a microcentrifuge. The process was repeated once, and finally an aliquot from the supernatant was transferred to 10 ml of scintillation mixture (Ecolume; ICN), and the radioactivity was determined by scintillation counting.

Enzyme Phosphorylation

Phosphorylation with ATP—Formation of the aspartyl-phosphate reaction intermediate was assayed as described (23), with some modifications. The 0.2-ml reaction mixture contained 25 mM Hepes/Tris, pH 7.0, 100 mM KCl, and 1 μg of purified Pmr1. To test cation dependence, EGTA was added to a final concentration of 1 mM such that the free Ca^{2+} concentration was less than 1 nM. Then 1 mM $CaCl_2$ or $MnCl_2$ was added to give free cation concentrations of 27 or 6 μM, respectively. The reaction was started by the addition of 10 μCi of [γ-^{32}P]ATP, to a final concentration of 10 nmol/reaction, on ice. The reaction was terminated after 30 s by adding 0.2 ml of 50 mM NaH_2PO_4, 2 mM ATP, and 20% trichloroacetic acid. The resulting precipitate was pelleted by microcentrifugation and washed twice with a solution containing 25 mM NaH_2PO_4, 1 mM ATP, and 10% trichloroacetic acid. The pellet was finally resuspended in 20 μl of sample buffer and subjected to SDS-polyacrylamide gel electrophoresis at pH 6.0 according to the method of Weber and Osborn (24). The gel was dried, and the radioactivity was detected on a PhosphorImager (Fuji).

Phosphorylation with P_i—Reverse phosphorylation of Pmr1 was performed according to Hawkins *et al*. (25). The reaction mixture of 0.2 ml contained 50 mM Hepes/Tris, pH 7.0, 100 mM KCl, 5 mM $MgCl_2$, 20% (v/v) dimethyl sulfoxide, and one of the following: EGTA (5 mM) or $CaCl_2$ or $MnCl_2$ (100 μM). Phosphorylation was initiated by the addition of 200 μM $^{32}P_i$ (1500–2000 cpm/pmol) at 25 °C for 5 min. The reaction was terminated by addition of 15% trichloroacetic acid and 2 mM KH_2PO_4 and incubated on ice for 15 min. After microcentrifugation, the pellet was treated as described for ATP-dependent (forward) phosphorylation and subjected to acid gel electrophoresis and autoradiography.

Gel Electrophoresis, Western Blotting, and Other Biochemical Assays

SDS-PAGE and Western blotting were performed as described previously (26). Samples were prepared for electrophoresis by precipitating with trichloroacetic acid to a final concentration at 10% by volume, followed by microcentrifugation at 4 °C. Antibodies against the C-terminal one-third of Pmr1 have been described previously (19). Silver staining was performed according to Blum *et al*. (27). Protein concentration was determined by a modification of the method of Lowry *et al.* (28).

Ab Initio Molecular Modeling of M4 and M6

A recently developed algorithm (29) was used to simulate packing of the M4 and M6 helices of Pmr1. Briefly, a reduced representation of the two helices was used in the first stage of modeling to simplify the search space. Each amino acid in a helix was considered to be a sphere with an empirically assigned volume that captures its packing attributes (30). The ball-helix representation used a simple model for the membrane bilayer, with the interior based on the Goldman-Engelman-Steitz transfer scale (31) and the interface based on the Wimley-White scale (32). Over 350,000 independent helix-pair combinations were explored to eliminate sterically "impossible" combinations. In the next stage, a more realistic representation of the membrane environment was applied, along with a more detailed protein representation. Finally, constraints were imposed based on experimental data from Cys cross-linking in SERCA (33) and mutagenesis of cation-coordinating residues in M4 and M6, as depicted in Fig. 8.

RESULTS

Purification of Histidine-tagged Pmr1

A 15-residue extension of the N terminus of Pmr1, having the sequence $RGSQH_9TR$ immediately following the initiating Met, was constructed in earlier work (13). We showed that introduction of this polyhistidine tag had no effect on the biogenesis and Golgi localization of Pmr1, as determined by subcellular fractionation of yeast lysates, and on the overall protein conformation, as evidenced by the pattern of ATP-

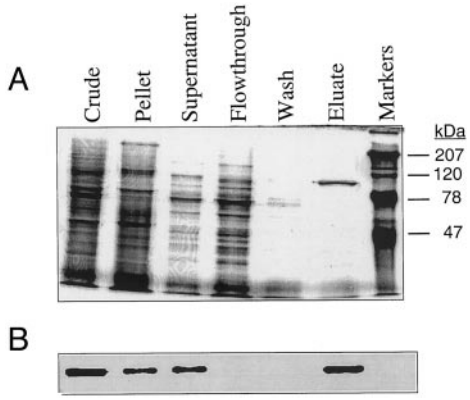

FIG. 1. **Solubilization and purification of histidine-tagged Pmr1.** Crude Golgi membranes were prepared from sucrose density gradients of yeast lysates solubilized with octylglucoside, and the supernatant was subjected to Ni-NTA chromatography, as described under "Experimental Procedures." 10-μg samples of crude, pellet, supernatant, column flowthrough, and wash and 1 μg of column eluate were separated by SDS-PAGE. Molecular mass markers are shown on the *far right*. *A*, silver-stained gel. *B*, Western blot probed with polyclonal anti-Pmr1 antibody.

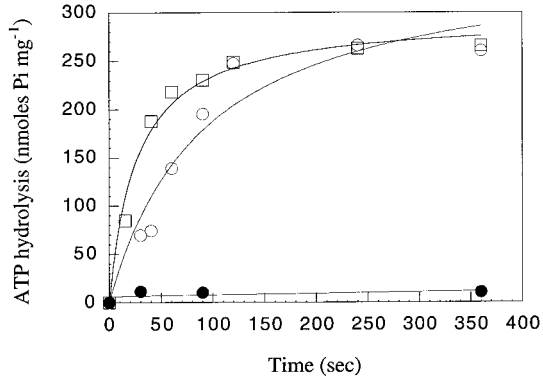

FIG. 2. **Time course of cation-dependent ATP hydrolysis.** Ni-NTA eluted Pmr1 (1 μg) was incubated with [γ-^{32}P]ATP (50 μM; 500 cpm/pmol) at room temperature for the indicated times, and the released $P0_4$ was quantitated as described in the text. $CaCl_2$ and $MnCl_2$ were at 950 μM each and buffered with 1 mM EGTA to give free cation concentrations of 6 μM each. Where indicated, $LaCl_3$ was added to a final concentration of 100 μM. □, Mn^{2+}; ○, Ca^{2+}; ●, Ca^{2+} plus La^{3+}. *Lines* are the best fit of the data to the Michaelis-Menten equation. Averages of duplicate determinations are shown, and data are representative of one of three independent experiments.

protectable tryptic cleavage (13). Furthermore, V_{max} and K_m for ^{45}Ca transport were identical to that reported earlier for untagged Pmr1 (13, 19). Here, we describe the purification of His-tagged Pmr1 by nickel affinity chromatography, in essentially one step. Golgi membrane fractions, derived from sucrose density gradient centrifugation of yeast lysates (19), were pooled and treated with the detergent *n*-octylglucoside, resulting in the solubilization of up to 70% of Pmr1 (Fig. 1). The supernatant was allowed to interact with Ni-NTA resin, as described under "Experimental Procedures." The inclusion of 10 mM imidazole during this incubation was found to greatly reduce nonspecific protein interactions with the resin while preserving complete retention of His-Pmr1. After washing the resin with salt and additional imidazole ("Experimental Procedures"), His-Pmr1 was eluted at >95% purity in buffer containing 300 mM imidazole, as judged from silver stains and Western blots of SDS-PAGE (Fig. 1). Yields of Pmr1 protein averaged 30 μg/liter of culture (approximately 600 OD units), consistent with an estimated expression level of about 5% in Golgi membranes.

Cation Dependence of Pmr1 Activity

ATP Hydrolysis—The availability of a purified preparation of Pmr1 allowed an unambiguous demonstration of cation-dependent ATP hydrolyis, using a sensitive isotope-based method ("Experimental Procedures"). ATPase activity was strictly dependent on the presence of either Mn^{2+} or Ca^{2+} and was linear within the first 30 s (Fig. 2). The presence of 500 μM vanadate (not shown) or 100 μM La^{3+} (Fig. 2) nearly abolished ATP hydrolysis, similar to the effect of these inhibitors on ATP-dependent ^{45}Ca transport in Golgi vesicles (19). No ATPase activity was observed with 10 μM concentrations of either Ba^{2+}, Sr^{2+}, Zn^{2+}, Cd^{2+}, Ni^{2+}, or Cu^{2+}, demonstrating the narrow cation selectivity profile of the pump.

Formation of the Phosphoenzyme Intermediate—A hallmark of P-type ATPases is the formation of a transient aspartyl-phosphate reaction intermediate, at an invariant aspartate located in the large hydrophilic domain closely following membrane span M4. Consistent with an obligatory role for this residue, we have shown that replacement of Asp^{371} in Pmr1 with asparagine or glutamate completely inactivates transport (19). Here, we demonstrate phosphoenzyme formation in the purified, His-tagged enzyme. In the forward reaction, formation of the E~P intermediate from ATP requires activation by either Ca^{2+} or Mn^{2+} (Fig. 3*A*). Addition of La^{3+} resulted in only modest increases in the accumulation of phosphoenzyme, unlike the large effect documented for plasma membrane type Ca^{2+}-ATPases (34). The aspartyl-phosphate intermediate could be completely chased with excess unlabeled ATP (Fig. 3*A*) and nonenzymatically cleaved with hydroxylamine (not shown). Conversely, in the reverse reaction, formation of E-P from inorganic phosphate (P_i) was inhibited by Ca^{2+} and

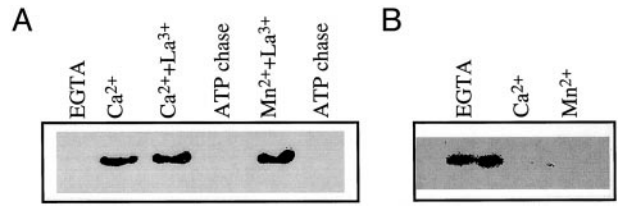

FIG. 3. **Formation of the phosphoenzyme intermediate.** *A*, Cation-dependent phosphoprotein formation from [γ-^{32}P]ATP. Ni-NTA eluted Pmr1 (1 μg) was incubated on ice for 30 s with 10 nM [γ-^{32}P]ATP in 20 mM Hepes/Tris, pH 7.0, 100 mM KCl, 1 mM EGTA, and 1 mM divalent cation, as indicated, to give a final free concentration of 27 μM Ca^{2+} and 6 μM Mn^{2+}. The reaction was stopped by acid quench and analyzed by SDS-PAGE and autoradiography. Where indicated, $LaCl_3$ was added to a final concentration of 100 μM. The E~P intermediate can be completely chased with unlabeled ATP (10 mM). *B*, cation-inhibitable phosphoprotein formation from P_i. The reaction differed from *A*, in having 250 μM [^{32}P]H_3PO_4 plus 20% dimethyl sulfoxide and was incubated at 25 °C for 5 min. Divalent cations were at 1 mM concentrations, as indicated.

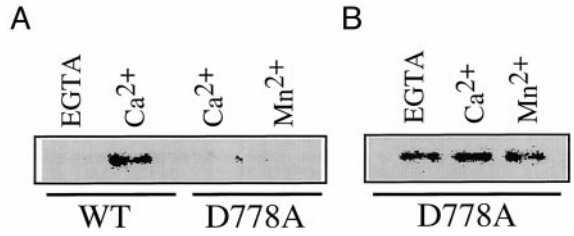

FIG. 4. **Loss of cation dependence of phosphoenzyme formation in the D778A mutant.** Wild type (*WT*) and D778A mutant Pmr1 were His-tagged, purified, and assayed for phosphoenzyme formation from [γ-^{32}P]ATP (*A*) or [^{32}P]PO_4 (*B*) as described under "Experimental Procedures" and the legend to *Fig. 3*. Ca^{2+} and Mn^{2+} fail to activate forward phosphorylation from ATP in the mutant or inhibit reverse phosphorylation from P_i, indicative of a defect in binding cations.

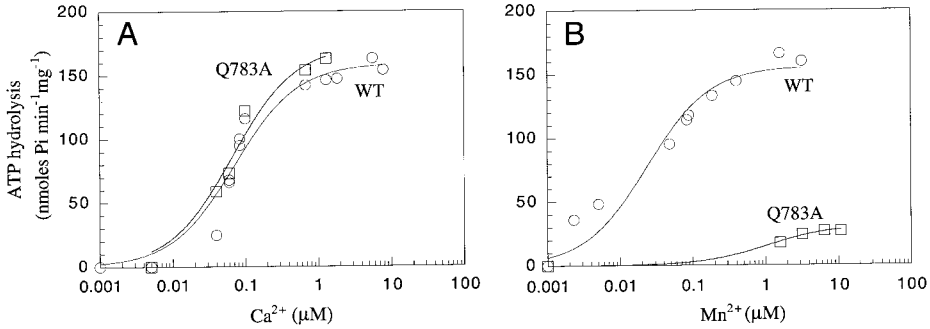

FIG. 5. **Selective loss of Mn^{2+}-dependent ATPase activity in the Q783A mutant.** His-tagged wild type (*WT*; ○) and mutant Pmr1 (*Q783A*; □) were purified by Ni-NTA chromatography and assayed for [γ-^{32}P]ATP hydrolysis in the presence of the free cation concentrations shown, as described in the text. *Symbols* are the average of duplicate determinations, and the *lines* represent the best fit of the data to the equation $v = V_{max}.S/(K_m + S)$ using Kaleidagraph, version 3. Derived values for K_m are reported in the text. Note the loss of Mn^{2+}-ATPase activity in the mutant, as predicted by the loss of Mn^{2+} tolerant growth (14).

Mn^{2+} (Fig. 3*B*), which shift the equilibrium toward the E_1 conformation.

Loss of Cation Binding in the D778A Mutant

Substitution of Asp^{778}, conserved in all known Ca^{2+}-ATPases, with either alanine, asparagine, or glutamate, resulted in a complete loss of transport activity consistent with the loss-of-function phenotype in screens of BAPTA and Mn^{2+} toxicity (14). However, to demonstrate a role for this residue in cation binding, it was necessary to examine cation-dependent formation of the catalytic intermediate. We first showed that mutant D778A was normal with respect to biogenesis, trafficking, and overall protein conformation (14). Next, mutant D778A was tagged with polyhistidine and purified, as described for wild type Pmr1. As expected, there was a complete absence of ATP hydrolysis in the purified mutant (not shown). Fig. 4 demonstrates an inability of this mutant to form the cation-activated phosphoenzyme intermediate from ATP, whereas reverse phosphorylation from inorganic phosphate is retained. Strikingly, reverse phosphorylation is insensitive to inhibition by cation (Ca^{2+} and Mn^{2+}), indicative of a loss of cation binding (15).

Loss of Manganese Selectivity in the Q783A Mutant

In the phenotypic screens reported earlier, mutant Q783A appeared similar to wild type in BAPTA tolerance but was indistinguishable from the *pmr1* null strain in Mn^{2+} tolerance, suggesting a selective loss of Mn^{2+} transport (14). Furthermore, Mn^{2+} inhibition of ^{45}Ca transport in Golgi vesicles was decreased by 60-fold, suggestive of a severe defect in Mn^{2+} binding or transport in this mutant (14). Here, we demonstrate a dramatic change in ion selectivity of the mutant pump by direct assay of cation-dependent ATPase activity in histidine-tagged and purified preparations of wild type and Q783A enzymes. Wild type Pmr1 displayed a K_m of 0.07 μM for Ca^{2+}-dependent ATP hydrolysis, identical to the K_m for ^{45}Ca transport reported earlier (13). Both K_m and V_{max} of Ca^{2+}-dependent ATPase activity in the Q783A mutant were essentially indistinguishable from wild type, as expected from the growth response to BAPTA in this mutant (Fig. 5*A*). Mn^{2+}-dependent ATPase activity in wild type had a K_m of 0.02 μM, indicative of a normal selectivity of $Mn^{2+} > Ca^{2+}$ for the Golgi/secretory pathway pump. In striking contrast, Mn^{2+}-ATPase in the mutant was nearly abolished (Fig. 5*B*). We also show normal levels of Ca^{2+}-activated phosphoenzyme formation from ATP in this mutant, whereas Mn^{2+} was required in excess (10 μM) to detect the catalytic intermediate (Fig. 6). Taken together, the data strongly indicate that residue 783 in M6 can define ion selectivity in Pmr1.

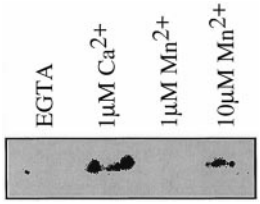

FIG. 6. **Selective loss of Mn^{2+}-dependent phosphoenzyme formation in the Q783A mutant.** Purified, His-tagged Q783A mutant Pmr1 (1 μg) was assayed for phosphoenzyme formation from [γ-^{32}P]ATP in the presence of EGTA (1 mM) or the free cation concentrations shown, as described in the text. Mn^{2+}-dependent E~P formation was detected only under the higher concentration of Mn^{2+} (10 μM), as shown.

Phenotypic Consequences of Amino Acid Substitutions at Residue 783 in M6

To further explore the effect of amino acid substitutions at position 783 on ion selectivity of the pump, additional mutations of Gln^{783} to Leu, Glu, Thr, Asn, Cys, and Ser were generated in the *PMR1* gene. These substitutions were chosen to test the effect of side chain size, hydrophobicity, or charge. Mutants were expressed from the low copy vector YCpHR1 in the *pmr1pmc1cnb1* null strain K616 and screened for tolerance to BAPTA and Mn^{2+} as a test of Ca^{2+} and Mn^{2+} transport, respectively (14). As shown in Fig. 7, only the Ala substitution resulted in a differential response to BAPTA and Mn^{2+} toxicity, indicative of a change in ion selectivity. Substitutions to Leu, Glu, or Thr showed substantial and parallel growth in both phenotypic screens, whereas substitutions to Asn, Ser, or Cys showed a hypersensitivity to BAPTA and Mn^{2+} toxicity indistinguishable from the *pmr1* null strain. Western analysis of total membrane preparations revealed that expression of the Leu, Glu, and Thr substitutions were similar to wild type, whereas substitutions to Asn, Ser, and Cys showed a significant decrease in abundance, suggestive of structural perturbations (not shown). These data reveal the importance of a bulky side chain (Gln, Leu, Glu, or Thr) at position 783 in M6 for effective transport of both Ca^{2+} and Mn^{2+} ions. Charge appears to be unimportant because both Leu and Glu can effectively substitute for Gln at this site. Conversely, introduction of a small, polar side chain at this site appears deleterious to pump structure and function. Interestingly, the small *non*polar side chain of alanine maintained normal pump structure but apparently altered pore characteristics such that Mn^{2+} transport was selectively lost.

DISCUSSION

Of the five polar or charged residues in transmembrane segment M6, three (Asn^{774}, Asp^{778}, and Gln^{783}) were found to

be critical for pump function (14). The importance of M6 is underscored by a striking conservation of sequence among Pmr1 homologues, which include representatives from four other fungi and one each from *C. elegans*, rat, and human; with the exception of an Ile substitution for Leu, there is complete identity within the predicted M6 segment. Of the three Ca^{2+}-liganding residues (Asn^{796}, Thr^{799}, and Asp^{800}) in M6 of SERCA, originally identified by Clarke *et al.* (15), two (Asn^{774} and Asp^{778}) are conserved and sensitive to substitution in the Golgi/secretory pathway ion pump. Replacement of the equivalent residues in the plasma membrane Ca^{2+} pump (plasma membrane Ca^{2+}-ATPase) have also been reported to inactivate transport and prevent phosphoenzyme formation from ATP (34, 35). Together with the conserved glutamate in M4 (Glu^{329} in Pmr1), these three residues are likely to contribute to the binding of one Ca^{2+} ion in all three Ca^{2+}-ATPase subtypes. In SERCA, this site would be equivalent to binding site II, the more cytoplasmic of two stacked sites (36, 37). A subset of these residues also appear to contribute to ion binding in P-type ATPases of different ion selectivities. Thus, Asp^{804} and Asp^{808} in M6 of the Na^+/K^+-ATPase have been proposed to play a key role in cation transport and in binding K^+ ions in particular (16). These observations have been corroborated by the mutagenesis of equivalent residues in the H^+/K^+-ATPase (38). The differential contribution of other residues to this common cation binding pocket may alter ion binding characteristics and account for the widely different ion selectivities among the P-ATPases. Thus, replacement of Ser^{775} in M5 of the Na^+/K^+-ATPase had a profound effect on K^+ binding (39), but mutation of the equivalent residue in Pmr1 (S774A) had no effect on Ca^{2+} or Mn^{2+} transport (14). Identifying the residues that contribute to ion selectivity remains a challenge in the field.

We report here that substitution of Gln^{783} with alanine results in a dramatic and selective loss of Mn^{2+}- but not Ca^{2+}-dependent ATPase activity and phosphoenzyme formation. We show that glutamine can be effectively replaced with either Leu (the equivalent residue in plasma membrane Ca^{2+}-ATPase) or Thr (the equivalent residue in SERCA), suggesting that Mn^{2+} transport may be a common feature of all Ca^{2+} pump subtypes. The restoration of Mn^{2+} tolerance to a *pmr1* mutant by heterologous expression of a plant homologue of SERCA, ECA1 (23), is consistent with this possibility. Curiously, introduction of an acidic residue (Glu) at this site preserved wild type phenotype, whereas small polar residues (Cys, Ser, or Asn) appeared to be deleterious to pump structure, based on the large reduction of Pmr1 expression levels. Because a helical representation of M6 placed Gln^{783} on the opposite face from the cation coordinating residues, we considered the possibility that this residue may be important in helix packing. Therefore, we simulated the packing interactions between transmembrane segments M4 and M6 ("Experimental Procedures"), using data from cysteine cross-links (33) to impose constraints on the models. Fig. 8 is an alignment of Pmr1 sequence with that of SERCA, showing the excellent conservation in the regions identified by strong cross-links between engineered Cys in transmembrane segments M4 and M6 of SERCA.

In a hierarchical approach to *ab initio* structure prediction,

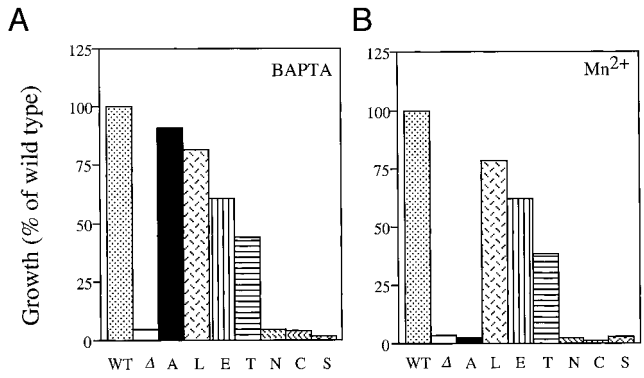

FIG. 7. **Phenotypic effects of substitutions at Gln^{783} on BAPTA and Mn^{2+} tolerance.** The host strain K616 (Δ*pmr1*Δ*pmc1*Δ*cnb1*) was transformed with vector alone (Δ) or low copy plasmids expressing wild type (*WT*) or mutant Pmr1 carrying the indicated substitution at position 783. Cultures were grown to saturation in media supplemented with BAPTA (*A*, 1.5 mM) or Mn^{2+} (*B*, 3 mM), as described (14). Growth (OD_{600}) was normalized to wild type. Only the Ala (*column A*) substitution showed differential sensitivity to BAPTA and Mn^{2+}. Substitutions to Leu (*column L*), Glu (*column E*), and Thr (*column T*) showed substantial and similar growth in both screens, whereas substitutions to Asn (*column N*), Cys (*column C*), and Ser (*column S*) showed no growth above the null background (Δ).

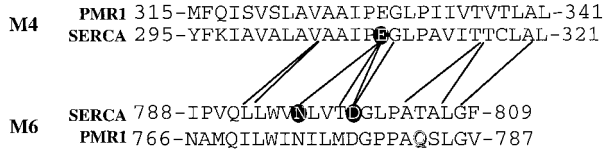

FIG. 8. **Alignment of Pmr1 and SERCA sequences in transmembrane segments M4 and M6.** *Circled* residues are proposed to coordinate cation in both SERCA and Pmr1. *Lines* show the locations of strong cross-links between engineered Cys in SERCA, as reported by Rice *et al*. (*33*). Gln^{783}, a residue that alters ion selectivity in Pmr1, is indicated as a *white letter* with *black outlines*. Note the excellent sequence conservation between SERCA and Pmr1 sequences in these segments.

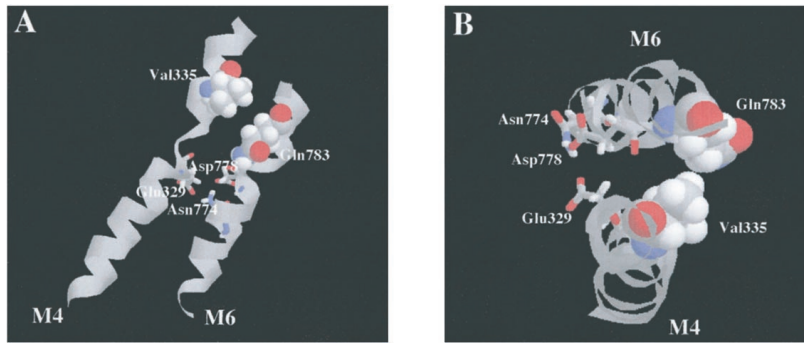

FIG. 9. **Molecular modeling of the packing interactions between transmembrane helices M4 and M6 of Pmr1.** A minimum energy conformation of the two helices is shown, modeled as described in the text. *A*, side view of the helices, shown labeled at their N termini, in which the side chains of Glu^{329} (M4), Asn^{774} and Asp^{778} (M6), proposed to form the cation binding pocket, are shown pointing away from the viewer. Gln^{783} (M6) is shown extending toward the viewer and appears to make a hydrophobic contact with Val^{335} (M4). *B*, top view of the helices showing Gln^{783} extending in a direction opposite to the proposed cation coordinating side chains, in close proximity to Val^{335}. Mutation Q783A is proposed to alter helix interaction and change the selectivity properties of the ion "pore" as described in the text.

we began with a reduced representation of the helices in which each amino acid was empirically assigned a spherical volume, characteristic of its packing attributes. Likewise, a reduced representation of the membrane environment was used ("Experimental Procedures") to simplify the search space. This allowed over 350,000 candidate conformations to be tested in the first stage, resulting in the elimination of all sterically impossible combinations. Following a second modeling stage that employed a more detailed protein and membrane representation, we imposed experimental constraints from Cys crosslinking and orientation of cation coordinating residues (Fig. 8). Of the dozen or so plausible models that emerged, Fig. 9 represents the minimum energy structure and has several interesting features. The helices interact with a right-handed twist, consistent with the interpretation of electron diffraction densities reported by Zhang *et al*. (40). Neither M4 nor M6 are uniform helices; both display a significant unraveling in the vicinities of the prolines, followed by a change in backbone direction. Of particular interest to this work is the location of Gln^{783} in the model. Fig. 9 suggests that Gln^{783} (M6) may form a hydrophobic contact with Val^{335} (M4), possibly stabilizing the helical interaction.

It should be emphasized that although our tertiary structure prediction does not take into account other transmembrane helices or consider significant deviations from helical structure, it does satisfy our currrent experimental observations and therefore provides a testable model for future experiments. Thus, it suggests that the hydrophobic interaction with Val^{335} may be maintained by the longer methyl- or methylene-containing side chains of Glu, Leu, or Thr but would be disrupted by introduction of shorter side chains carrying the polar amine (Asn), sulfhydryl (Cys), or hydroxyl (Ser) groups. Alanine substitution may maintain the hydrophobic interaction but with likely alterations in helix packing. We suggest that these changes would have repercussions on the architecture of the ion pore and hence on ion selectivity. The arrangement and tilt of the helices may be expected to have a profound effect on ion selectivity, as suggested by the recent structure of the KcsA K^+ channel (41). In experiments currently underway in our laboratory, we are engineering reciprocal alterations in M4 in an attempt to suppress the Mn^{2+}-sensitive phenotype of Pmr1 mutant Q783A.

REFERENCES

1. Loukin, S., and Kung, C. (1995) *J. Cell Biol.* **131,** 1025–1037
2. Durr, G., Strayle, J., Plemper, R., Elbs, S., Klee, S. K., Catty, P., Wolf, D. H., and Rudolph, H. K. (1998) *Mol. Biol. Cell* **9,** 1149–1162
3. Osterberg, R. (1974) in *Metal Ions in Biological Systems: High Molecular Complexes* (Siegel, H., ed) Vol. 3, pp. 45–88, Marcel Dekker, Inc., New York
4. Lawrence, G. D., and Sawyer, D. T. (1978) *Coordination Chem. Rev.* **27,** 173–193
5. Williams, R. J. P. (1982) *FEBS Lett.* **140,** 3–10
6. Reed, G. H. (1986) in *Manganese in Metabolism and Enzyme Function* (Schramm, V. L., and Wedler, F. C., eds) pp. 313–323, Academic Press, Inc., San Diego, CA
7. Kawasaki, H., Kuroso, Y., Kasai, H., Isobe, T., and Okuyama, T. (1986) *J. Biochem.* (*Tokyo*) **99,** 1409–1416
8. Keller, C. H., LaPorte, D. C., Toscano, W. A., Jr., Storm, D. R., and Westcott, K. R. (1980) *Ann. N. Y. Acad. Sci.* **356,** 205–219
9. Wilson, S. P., and Kirshner, M. (1983) *J. Biol. Chem.* **258,** 4994–5000
10. Loneragan, J. F. (1988) in *Manganese in Soil and Plants* (Graham, R. D., Hannam, R. J., and Uren, N. C., eds) pp. 113–124, Kluwer Academic Publishers, Dordrecht, The Netherlands
11. Luckhoff, A., and Clapham, D. E. (1992) *Nature* **335,** 356–358
12. Lapinskas, P. J., Cunningham, K. W., Liu, X. F., Fink, G. R., and Culotta, V. C. (1995) *Mol. Cell. Biol.* **15,** 1382–1388
13. Wei, Y., Marchi, V., Wang, R., and Rao, R. (1999) *Biochemistry* **38,** 14534–14541
14. Wei, Y., Chen, J., Rosas, G., Tompkins, D. A., Holt, P. A., and Rao, R. (2000) *J. Biol. Chem.* **275,** 23927–23932
15. Clarke, D. M., Loo, T. W., Inesi, G., and MacLennan, D. H. (1989) *Nature* **339,** 476–478
16. Kuntzweiler, T. A., Arguello, J. M., and Lingrel, J. B (1996) *J. Biol. Chem.* **271,** 29682–29687
17. Cunningham, K. W., and Fink, G. R. (1994) *J. Cell Biol.* **124,** 351–363
18. Fisher, C. L., and Pei, G. K. (1997) *BioTechniques* **23,** 570–574
19. Sorin, A., Rosas, G., and Rao, R. (1997) *J. Biol. Chem.* **272,** 9895–9901
20. Fu, D., and Maloney, P. C. (1997) *J. Biol. Chem.* **272,** 2129–2135
21. Ghosh, J., Ray, M., Sarkar, S., and Bhaduri, A. (1990) *J. Biol. Chem.* **265,** 11345–11351
22. Bers, D., Patton, C., and Nuccitelli, R. (1994) *Methods Cell Biol.* **40,** 3–29
23. Liang, F., Cunningham, K. W., Harper, J. F., and Sze, H. (1997) *Proc. Natl. Acad. Sci. U. S. A.* **94,** 8579–8584
24. Weber, K., and Osborn, M. (1969) *J. Biol. Chem.* **244,** 4406–4412
25. Hawkins, S. C., Xu, A., and Narayanan, N. (1994) *Biochem. Biophys. Acta* **1191,** 231–243
26. Nakamoto, R. K., Rao, R., and Slayman, C. W. (1991) *J. Biol. Chem.* **266,** 7940–7949
27. Blum, H., Beier, H., and Gros, H. J. (1987) *Electrophoresis* **8,** 93–99
28. Lowry, O. H., Rosebrough, N. J., Farr, A. L., and Randall, R. J. (1951) *J. Biol. Chem.* **193,** 265–275
29. Woolf, T. B., Grossfield, A., and Sachs, J. N. (2000) *Biophys. J.* **78,** 159 (abstr.)
30. Pontius, J., Richelle, J., and Wodak, S. J. (1996) *J. Mol. Biol.* **264,** 121–136
31. Engelman, D. M., Steitz, T. A., and Goldman, A. (1986) *Annu. Rev. Biophys. Chem.* **15,** 321–353
32. Wimley, W. C., and White, S. H. (1996) *Nature Struct. Biol.* **3,** 842–848
33. Rice, W. J., Green, N. M., and MacLennan, D. H. (1997) *J. Biol. Chem.* **272,** 31412–31419
34. Adebayo, A. O., Enyedi, A., Verma, A. K., Filoteo, A. G., and Penniston, J. T. (1995) *J. Biol. Chem.* **270,** 27812–27816
35. Guerini, D., Foletti, D., Vellani, F., and Carafoli, E. (1996) *Biochemistry* **35,** 3290–3296
36. Skerjanc, I. S., Toyofuku, T., Richardson, C., and MacLennan, D. H. (1993) *J. Biol. Chem.* **268,** 15944–15950
37. Andersen, J. P., and Vilsen, B. (1994) *J. Biol. Chem.* **269,** 15931–15936
38. Swarts, H. G., Klaassen, C. H., de Boer, M., Fransen, J. A., and De Pont, J. J. (1996) *J. Biol. Chem.* **271,** 29764–29772
39. Blostein, R., Wilczynska, A., Karlish, S. J. D., Arguello, J. M., and Lingrel, J. B. (1997) *J. Biol. Chem.* **272,** 24987–24993
40. Zhang, P., Toyoshima, C., Yonekura, K., Green, N. M., and Stokes, D. L. (1998) *Nature* **392,** 835–839
41. Doyle, D. A., Cabral, J. M., Pfuetzner, R. A., Kuo, A., Gulbis, J. M., Cohen, S. L., Chait, B. T., and MacKinnon, R. (1998) *Science* **280,** 69–77